On the Multiferroic properties of single phase $Bi_{0.85}Ho_{0.05}Sm_{0.1}FeO_3$ ceramics.

rajesh[1], S. John Ethilton[1], K. Ramachandran[2], N. V. Giridharan[3], K. Rameshkumar[4], and Samba Siva Vadla[5]

[1]Velammal College of Engineering & Technology, Madurai 625 009, India
[2]Gandhigram Rural Institute Deemed University, Dindigul, India
[3]National Institute of Technology, Tiruchirapalli, India
[4]Department of Physics, University of Johannesburg, South Africa
[5]Indian Institute of Technology Madras, Chennai, India

February 11, 2018

Abstract

For the first time, magnetoelectric and multiferroic properties of single phase polycrystalline $Bi_{0.85}Sm_{0.1}Ho_{0.05}FeO_3$ ceramic is reported here. $BiFeO_3$, $Bi_{0.9}Sm_{0.1}FeO_3$ and $Bi_{0.85}Sm_{0.1}Ho_{0.05}FeO_3$ are prepared by conventional solid-state route. The Rietveld refinement analysis explains the occurrence of distortion in rhombohedral phase with respect to host $BiFeO_3$. The remanent polarization and hence magnetization of $Bi_{0.85}Sm_{0.1}Ho_{0.05}FeO_3$ ceramic are found to be significantly improved to some extent than $BiFeO_3$ and $Bi_{0.9}Sm_{0.1}FeO_3$. Magnetic field coupled to ferroelectric loop tracer and temperature dependent dielectric permittivity shows the signature of magnetoelectric coupling present in the sample.

Keywords: Multiferroics, Magnetization, Ferroelectrics and Magnetoelectric coupling

***corresponding author email: rr@vet.ac.in Telephone: +91 452 2465289 (Extn: 208)**

1. Introduction

Materials possessing multiferroic properties have potential applications in information storage, sensors, spintronics, etc. Even though there are many multiferroic materials now available, $BiFeO_3$ stands distinct in the sense that there is strong coupling between ferroelectricity and ferromagnetism. $BiFeO_3$ is of current interest for researchers, as magnetic and ferroelectric orderings are possible above room temperature. But practical applications of this material have many limitations. So, doping or co-doping in this $BiFeO_3$ is being tried nowadays to make it successful for multiferroic applications. Amit Kumar and Yadav [Kumar and Yadav (2013)] have studied the enhancement of magnetoelectric properties *La*, *Lu* co-doped BiFeO3 as BiFeO3 is a known magnetoelectric material. They have also added small quantity of *La* at *Bi* site to reduce the Bi3+ volatilization and oxygen vacancies. With this, they could report an enhancement in the magnetoelectric capacitance is nearly three times the bare BiFeO3. Due to the ferroelectric Curie temperature of Tc ~ 830 ^0C and G-type antiferromagnetic Neel Temperature (TN) of 370 ^0C, on doping with *La* and *Lu*, it is found that T_N shifts towards lower temperature, thereby room temperature coupling is possible. This also makes it as a useful material for practical applications.

Recently in 2017, Abdelkafi *et al* [(**Abdelkafi et al., 2017**)] have report dielectric relaxation study in *Ni*, *Ti* co-doped $BiFeO_3$ at *Fe* site. The dielectric anomaly at 247 *C* near the Neel temperature (T_N) supports the strong magnetoelectric coupling. Among the various methods, the method of doping is found to be successful to modify the crystal structure and tune the physical properties.

Most of the reported studies on divalent ion doped BiFeO3 have focussed on the investigation of modifications in the crystal structure and the corresponding changes in magnetization and electric polarization [(**Tirupathi and Chandra, 2013**)]. Rarely reported the results of dielectric constant changes near the magnetic transition. These works lead to the present investigation on the multiferroic properties of *Ho*, *Sm* co-doped BiFeO3 at *Bi* site.

2. Experimental Details

2.1. Synthesis

Polycrystalline BiFeO3, Bi0.9Sm0.1FeO3 and Bi0.85Sm0.1Ho0.05FeO3 are prepared by high temperature solid

state reaction. High purity powders such as Bi2O3, Fe2O3, Sm2O3 and Ho2O3 (99.99% pure from Sigma Aldrich & Alfa Aesar) are taken in the stoichiometric ratio and ground vehemently with mortar & pestle made of agate for *30* minutes for homogeneity. Then these mixed powders were calcined in two step process at 600° *C* for 2 *hours* and then at 835° *C* for 2 *hours* with intermediate grinding and consequently quenched towards room temperature to avoid oxygen deficiency [(**Zhang et al., 2005**)]. These residues of mixed powders are pelletized using polyvinyl alcohol as a binder. Three distinct cylindrical pellets are prepared by a hydraulic press at 30 *MPa*. These pellets were then sintered finally at 835° *C* for 2 *hours* at the rate of 10 °*C / minute* with an accuracy of 0.02 °*C*. Finally, the sintered pellets were coated with silver paint.

2.2. Characterization

Phase identification of the samples is examined from the powder X-ray diffraction (XRD) using PANalytical X'Pert Pro Plus Goniometer PW3050/60 X-ray diffractometer with ŭKα radiation in a wide scanning range of 10° to 90° with a step size of 0.0170. Rietveld refinement on XRD pattern is performed using GSAS II (General Structure Analysis System) software to analyse the crystallographic structure present in the sample. The surface morphology of the sample is investigated using FEG quanta 250 scanning electron microscope (SEM).

Temperature dependent dielectric analysis is done for frequencies of 1 *Hz* to 107 *Hz* at the temperature of 30° *C* to 500° *C* using Alpha A impedance analyser (Novocontrol, Germany). Ferroelectric hysteresis loops of the samples are measured using Precision Premier II Multiferroic test system (Radiant Technology, USA). The leakage current of the samples is measured using Keithley 6517 electrometer. Magnetoelectric measurements are observed using Polytronic electromagnet HEM 100along with Lakeshore 425 Gaussmeter up to a field of 9 *kOe* and magnetization measurement by using Lakeshore VSM7410 vibrating sample magnetometer.

3. Results and Discussion

3.1. Structural and microstructural analysis

The X-ray diffraction patterns of BiFeO3, Bi0.9Sm0.1FeO3 and Bi0.85Sm0.1Ho0.05FeO3 at ambient temperature are shown in **Fig** 1. BiFeO3 reveal the formation of Rhombohedral *R3c* structure with minor secondary phases such as Bi2Fe4O9 and Bi25FeO40 [(Catalan and Scott, 2009)]. The three samples shows distant separation of (1 0 4) and (1 1

0) planes with variation in intensities and hence are remained in same *R3c* phase (JCPDS# 01-086-1518) based on the crystal structure of BiFeO3

Compare with BiFeO3, due to the substitution of *Sm* in BiFeO3, the intensity of secondary phases (Bi2Fe4O9 & Bi25FeO40) are diminished and the peak intensities of (1 0 4) plane is decreased compared to (1 1 0) plane indicating a slight structural distortion in *R3c* phase than BiFeO3 (2). As a result the volume of the unit cell slightly reduces. This trend is similar to the x- ray diffraction patterns observed by sati *et al* [(Sati et al., 2014)].

Further, adding 5% of *Holmium* on *Sm* doped BiFeO3 eliminates the secondary phases arising from pristine BiFeO3 and shift the peak intensities to higher angles (**Fig** 2). Similar results are reported in few of the modified *A* - site doped BiFeO3 ceramic[(Sati et al., 2014)(Kumar and Yadav, 2013)]. This shift in peak intensities conform the substitution effect of Ho3+ on *Sm* doped BiFeO3 and results in significant structural distortion on the crystal structure of Bi0.85Sm0.1Ho0.05FeO3.

The Goldschmidt tolerance factor is used to examine the structural stability of the compounds given by

$t = \frac{<r_A>+r_0}{r_B+r_0}$ (1) Where $<r_A>$ is the average radius of Bi^{3+}, Sm^{3+} and Ho^{3+} ions at *A* site and r_B and r_0 are the radius of Fe^{3+} and O^{2-} ions respectively. The tolerance factor of BiFeO3, Bi0.9Sm0.1FeO3 and Bi0.85Sm0.1Ho0.05FeO3 are found to be 0.889, 0.884 and 0.881 respectively. Since the tolerance factor of Bi0.85Sm0.1Ho0.05FeO3 is comparatively minimum and less than unity, since the tolerance factor is minimum and less than unity in Bi0.85Ho0.05Sm0.1FeO3, it is expected that during co - doping, the influence of short range trivalent metal ions such as Ho^{3+} and Sm^{3+} are compensated by long range Bi^{3+} ions with minimum lattice strain. The shift in XRD peaks around 51°, 57° supports the substitution in Bi0.85Sm0.1Ho0.05FeO3.

Fig 3 & 4 shows the Rietveld refinement of the powder diffraction pattern using GSAS II (General Structure Analysis System II) with least square algorithms[(Toby and Dreele, 2013)] . Bi0.85Sm0.1Ho0.05FeO3 is indexed well in *R3c* phase with the acceptable goodness of fit(GOF), *R*-structure factor(R_f), *R*-Bragg factor(R_b), *R*-pattern factor (R_p)and weight profile factor (WR_p) values. The normal probability plots for the distribution of error in the experimental X-ray diffraction is calculated from error analysis using Bayesian fits and differences normalized by the corresponding values of the estimated standard deviations, ranges, slope and their intercepts[(Gagin and Levin, 2015)]. The Rietveld refined parameters of all the samples are listed in the Table 1 and are shown in Fig. 3 & 4. From Rietveld results, the bond angle of BiFeO3 (Fig. not shown), Bi0.9Sm0.1FeO3 and Bi0.85Ho0.05Sm0.1FeO3 along [111] direction are found to be 154.139°(0), 154.760°(0) and 155.062°(1) respectively. The tilt angle of FeO6 octohedra tilt angle can be calculated using the relation

$$\cos\ \theta_1 = \frac{2\ -5\ \cos^2\phi_1}{2+\cos^2\phi_1} \quad (2)$$

$$\cos\ \theta_2 = \frac{1-4\ \cos^2\phi_1}{3} \quad (3)$$

where ϑ1 and ϑ2 are the two Fe - O - Fe angles related to tilt angle φ of the FeO6 octohedra around pseudocubic [111] directions [(Chatterji et al., 2002)]

The tilt angles (φ) of FeO6 octohedra were calculated for BiFeO3, Bi0.9Sm0.1FeO3 and Bi0.85Ho0.05Sm0.1FeO3 samples and found to be 15.54°, 15.52° and 15.33° respectively. According to Nayek *et al*, the canting of Fe3+ ions in BiFeO3 is understood from antisymmetric Dzyaloshinskii Moriya (DM) exchange energy[(Nayek et al., 2014)]. i.e., for any rare earth substituted BiFeO3, Fe - O - Fe bond angle is deviated from the ideal pervoskite angle (180°) because of the DM exchange energy between Fe ions and favours spin canting [(Nayek et al., 2014)]. Hence it is expected that the magnetic behaviour will be altered in Bi0.85Ho0.05Sm0.1FeO3 with respect to Bi0.9Sm0.1FeO3 and BiFeO3

The Surface morphology of BiFeO3, Bi0.9Sm0.1FeO3 and Bi0.85Ho0.05Sm0.1FeO3 ceramics are shown in Fig. 5 & 6 . From the SEM images, it is observed that all the samples are crystallizes in micrograins range. The average particulate size were estimated to be pristine BiFeO3 is found to be 1.17 μμ. Whereas the particulate sizes of Bi0.9Sm0.1FeO3 and Bi0.85Ho0.05Sm0.1FeO3 possess a non-uniform grains with decrease in grain size and increase in grain boundaries than BiFeO3. The decrease in grain size may be due to the reduction of oxygen vacancies in FeO6

octahedral site. However, Bi0.85Ho0.05Sm0.1FeO3 image exhibits voids of irregular dimension due to presence of porosity which might reduce the density in the ceramics [(**Pattanayak et al., 2013**)]

3.3. Magnetic studies

Fig.7 shows magnetization as a function of magnetic field (M - H) for BiFeO3, Bi0.9Sm0.1FeO3 and Bi0.85Sm0.1Ho0.05FeO3 at ambient temperature. The magnetization curves of all the samples are varying up to 15 *kOe* specifying an antiferromagnetic ordering with corkscrew modulated spin structure. The magnetization values at magnetic field of 15 *kOe* for BiFeO3, Bi0.9Sm0.1FeO3 and Bi0.85Sm0.1Ho0.05FeO3 are found to be 0.088 *emu /g*, 0.1616 *emu /g*, and 0.2370 *emu /g* respectively.

BiFeO3 is known to be a weak antiferromagnetic substance with canted spin structure. Significant increase of magnetization in Bi0.9Sm0.1FeO3 and Bi0.85Sm0.1Ho0.05FeO3 ceramic are due to partial suppression of spiral spin ordering and results in the variation of Fe - O - Fe canting angle [(**Karthik et al., 2012**)]. Because ruette *et al* shows that the modulated spiral spin ordering gets completely destroyed at a magnetic field of 18 *T* (i.e., 180 *kOe*). Here, the magnetization values are observed at a maximum field of 1.5 T (15 *kOe*). This conforms the partial suppression of spiral spin ordering [(Ruette et al., 2004)].

On the other hand, the magnetization behaviour of Bi0.85Sm0.1Ho0.05FeO3 ceramic gets considerably enhanced than other two ceramics. This is because, Ho3+ is known to be magnetically active ion and comparatively the ionic radii of Ho3+ is smaller than Bi3+ and Sm3+ ions. Hence 5% of Holmium added to *Sm* doped BiFeO3 ceramics might experience a interaction between Fe3+ and Ho3+ ions in octahedral site and decouples the antiferromagnetic interactions with Fe3+ ions to some extent. As a result, the magnetization values gets improved. These results are comparable with some of the alkali rare earth doped polycrystalline ceramics [(**Zhang et al., 2011**)].

Further the remanent magnetization (2Mr) of BiFeO3, Bi0.9Sm0.1FeO3 and Bi0.85Sm0.1Ho0.05FeO3 are found to be 0.0021 *emu /g*, 0.0387 *emu /g*, and 0.0439 *emu /g* respectively, According to Kumar *et al* and karthick *et al*, the increase in Mr value may be due to the suppression of spiral spin ordering and coexistence of antiferromagnetic and weak ferromagnetic orderings [(**Karthik et al., 2012**)(**Uniyal and Yadav, 2009**)] In order to justify the favouring of magnetic ordering (ferro magnetic or antiferromagnetic) in BiFeO3, Bi0.9Sm0.1FeO3 and Bi0.85Ho0.05Sm0.1FeO3 ceramics, Arrott - Belov - Kouvel (*ABK*) plots are drawn which is based on Weiss molecular field theory [(**Singh et al., 2013**)]. *ABK* plots are analysed using a linear function and then extrapolated to get Y intercept which is considered as saturation magnetization (Ms). If the Y intercept at H = 0 is negative, then contribution of antiferromagnetic ordering is favoured in the ceramics. Instead, if the Y intercept at H= 0 axis is positive, then the contribution of ferromagnetic ordering is favoured. Fig. 8 shows ABK plots of all the three samples at ambient temperature. The ABK plot reveals a negative Y intercept without any spontaneous magnetization at H = 0, representing an antiferromagnetic ordering is favoured in all the three ceramics [(**Kumar et al., 2015**)].

3.4. Dielectric studies

Fig. 9 and the inset of 9 shows frequency dependent dielectric constant and dielectric loss of BiFeO3, Bi0.9Sm0.1FeO3 and Bi0.85Sm0.1Ho0.05FeO3 at ambient temperature. Initially, dielectric constant are higher at lower frequencies and start decreasing on increasing the frequencies in all the three samples. Finally all of them are approaching towards constant value at higher frequencies. The high value of dielectric permittivity at lower frequencies are due to charge accumulation at grain boundaries. The extremely large permittivities/losses accompanied by a strong dispersion are due to charged defects such as vacancies which contribute to the interfacial polarization due to the Maxwell-Wagner effect. [(**Suresh et al., 2016**)]. The dielectric constants at 1 *MHz* for BiFeO3, Bi0.9Sm0.1FeO3 and Bi0.85Sm0.1Ho0.05FeO3 are found to 26, 79 and 50 which is comparable with some of the alkali rare earth doped polycrystalline ceramics [(Hussain et al., 2015) (Muneeswaran et al., 2015)]. Comparing the dielectric constant value of pristine BiFeO3 with Bi0.85Sm0.1Ho0.05FeO3, high values of *er* is observed which may be ascribed due to the

suppression of secondary phases and/ or due to the presence of oxygen vacancies in FeO6 octahedral site. The dielectric loss at 1 *MHz* for BiFeO3, Bi0.9Sm0.1FeO3 and Bi0.85Sm0.1Ho0.05FeO3 are found to 0.268, 0.429 and 0.206 respectively. The value of dielectric loss for Bi0.85Sm0.1Ho0.05FeO3 ceramic is comparatively lower than other ceramics because of the reduction of Fe2+ ions in Fe3+ / Fe2+ redox couple which might reduce the conductivity and losses values [(SINGH et al., 2004)].

Fig 10 and the inset of Fig. 10 shows temperature dependent dielectric permittivity and the tangent loss of Bi0.85Ho0.05Sm0.1FeO3 ceramic in the frequency range to 5 *kHz* to 5 *MHz* respectively. Temperature dependent dielectric permittivity (er') at different frequencies shows strong dispersion over the measured temperature ranges. For the measured wide region, two anomalies are observed in Bi0.85Ho0.05Sm0.1FeO3 ceramics. Anomaly at 290° *C* corresponding to Neel temperature (T_N) and other at 481° *C* corresponding to Curie temperature (Tc). The observed dielectric anomaly around T_N may arise because of different reasons such as (i) resistive component of dielectric behaviour along with Maxwell - Wagner effect [(**Catalan, 2006**)] (ii) intrinsic magneto electric coupling due to the vanishing magnetic order over the electric order as predicted by Landau - Devonshire theory of phase transition [(Benguigui, 1972)]. In order to verify the origin of anomaly in er'(T), temperature dependent resistivity across TN is also measured between 1 *kHz* to 1 *MHz* as shown in Fig. 11. The observed results clearly pointing out that, there is no anomaly in the DC resistivity curve especially at the Neel temperature (TN) range and conforms the anomaly in temperature dependent dielectric constant is due to the intrinsic magnetoelectric coupling in Bi0.85Ho0.05Sm0.1FeO3 ceramics.

In case of temperature dependent dielectric loss (ταν δ), the value of ταν δ is low at lower temperatures and start increasing as the temperature increases. Around 200° *C*, the dielectric loss decreases rapidly as the frequency increases from 5 *kHz to* 5 *MHz* which is attributed to the influence of conductivity behaviour triggered by the presence of Fe2+ ions in the sintered Bi0.85Ho0.05Sm0.1FeO3 ceramics [(**Abdelkafi et al., 2017**)]. Also, high value of dielectric loss at higher frequencies is ascribed to the presence of coexistence of Fe2+ and Fe3+ ions in octahedral sites due to electron hopping conduction mechanism and presence of oxygen vacancies originating from the volatile nature of Bi3+ and / or transition from Fe3+ to Fe2+ ions [(**SINGH et al., 2004**)].

3.5. Ferroelectric and leakage current studies

Fig. 12 shows the ambient temperature electric field dependence of polarization (*P* - *E*) of polycrystalline BiFeO3, Bi0.9Sm0.1FeO3 and Bi0.85Sm0.1Ho0.05FeO3 ceramics at *100 Hz*. The *P* - *E* loops of all the ceramics shows a loosy trend which might be due to presence of leakage current. However, the shape of *P* - *E* loop is significantly improved in Bi0.85Sm0.1Ho0.05FeO3 compare to the Bi0.9Sm0.1FeO3 and BiFeO3 samples and showing a nearly saturated ferroelectric behaviour to some extent. The remanent polarization (Pr) of BiFeO3, Bi0.9Sm0.1FeO3 and Bi0.85Sm0.1Ho0.05FeO3 are 0.0126 μ̂ / ς μ2, 0.045 μ̂ / ς μ2 and 0.0753 μ̂ / ς μ2 respectively. This means that the ferroelectric behaviour is considerably enhanced by *Holmium* doping on *Sm* doped BiFeO3 ceramics. These results are comparable and better than some of the rare earth doped BiFeO3 either in nano or polycrystalline bulk form [(**Muneeswaran et al., 2015**)]. From these observations, it is found that the ferroelectric behaviour is considerably increased in Bi0.85Sm0.1Ho0.05FeO3 ceramic.

Fig.13 shows the leakage current density of BiFeO3, Bi0.9Sm0.1FeO3 and Bi0.85Sm0.1Ho0.05FeO3 ceramics at ambient temperature. From *J* - *E* curves, it is found that at an applied field of 20 *kV/cm*, the leakage current density of Bi0.85Sm0.1Ho0.05FeO3 is 5.753 x 10-10 *A / cm2*, which is approximately one order and three orders less in magnitude than Bi0.9Sm0.1FeO3 (3.83 x 10-9 μ̂ / ς μ2) and BiFeO3 (1.87 x 10-7 μ̂ / ς μ2) hence the leakage current density of Bi0.85Sm0.1Ho0.05FeO3 is decreased on substituting Holmium content in *Sm* doped BiFeO3 ceramic [(**Zhang et al., 2011**)]. The reason behind reduced leakage current and higher remanent polarization are may be due to the reduction of oxygen vacancies which might induce the pinning effect on polarization switching domains thereby improving the ferroelectric properties [(**Mao et al., 2011**)].

3.6. Magnetoelectric coupling

The change in magnetization for an applied electric field or of polarization by magnetic field leads to magnetoelectric effect**.** This coupling effect is demonstrated by measuring the *P-E* loop of Bi0.85Sm0.1Ho0.05FeO3 ceramic at a particular frequency, with static magnetic field.

Here the polarization and hence the dielectric constant are found to be varying with applied magnetic fields.

The dielectric behaviour of the sample in the presence of magnetic field leads to the magnetodielectric (*MD*) effect and can be expressed as [(Zhang et al., 2011)(Dai et al., 2016)].

$$MD = \frac{\epsilon(H)-\epsilon(0)}{\epsilon\ (0)} \cdot 100\% \tag{4}$$

where & are the dielectric constant with presence and absence of the magnetic field. The value of magnetodielectric effect at a frequency of 100 *Hz* is increased for increasing magnetic field (Fig. 14) and the coupling coefficient is found to be 0.91 % at 4 *kOe*. This is because, whenever there is a rotation of oxygen octahedron, the tilt angle gets varied and favours Dzyaloshinskii-Moriya (*DM*) magnetic moments which results in increasing the intrinsic spin lattice coupling [(**Tirupathi and Chandra, 2013**)]. Further, in order to conform the presence of magnetoelectric coupling in Bi0.85Sm0.1Ho0.05FeO3 ceramic, Magnetic poling was performed on this ceramics at ambient temperature as shown in Fig. 15. After 25 minutes of poling under 9 *kOe* of *DC* magnetic field, the remanent polarization (*2Pr*) changes from 0.18 μ̂ / ς̂μ2 to 0.11 μ̂ / ς̂μ2. Also, the area of *P - E* loop before and after pooling (9 *kOe*) of magnetic field are found to be 1.06% and 0.64%. This clear change in the area of *P - E* loop conforms the signature of magnetoelectric coupling present in the ceramic. Similar trend was already identified by Tirupathi *et al* for Bi1-xCaxFeO3 ceramics. Here, the magnetoelectric coupling appears on Bi0.85Sm0.1Ho0.05FeO3 ceramic is based on the qualitative explanation put forward by Palkar *et al* [(**Palkar et al., 2004**)]. According to Palkar *et al*, when magnetic field is applied to multiferroic material, due to the coupling between magnetic and ferroelectric domains, the material will be strained. As a result, this strain induces a stress in the ferroelectric domain and tempts an electric field in the material. Therefore the polarization and dielectric constant varies accordingly.

4. Discussion

BiFeO3 is known to an interesting material for the reasons that it is found to be a multiferroic as well as magnetoelectric. All magnetoelectric materials need not be multiferroic and vice versa. Literature shows that a partial substitution of trivalent metal ions like Sm3+[(Khomchenko et al., 2010)], La3+(Jangid et al., 2012), Dy3+(Muneeswaran et al., 2015) ,Ho3+(Rao et al., 2012) and Gd3+(Pattanayak et al., 2013) would distort the crystal structure of the host BiFeO3 to enhance the multiferroic ordering. Also, as the doping concentration of trivalent metal ions exceeds 15% in BiFeO3 most of the system involves a structural phase transformation

Eventhough there are number of articles in single phase *Sm* doped BiFeO3 ceramics with enhanced multiferroic behaviours due to structural changes, particularly due to the change in bond length and reduced secondary phases. Here, we went for co-doping because as *Sm* doped BiFeO3 shows strong signature of secondary phases in XRD analysis and may violate the aim. Now when both *Sm* and *Ho* trivalent ions are substituted at *Bi* site (in very small concentration), it is found that it retains the structure of host BiFeO3 reducing all the secondary phases. Here the role of Ho3+ is not only to enhance the multiferroic behaviour but also to supress the secondary phases and to reduce the high leakage current density. (Uniyal and Yadav, 2009; Zhang et al., 2011; Kumar and Yadav, 2013) .

5. Conclusion

Single phase polycrystalline Bi0.85Sm0.1Ho0.05FeO3 is successfully prepared through solid state route and the variation of bond angle and bond length influencing the electrical and magnetic properties are investigated from Rietveld refinement analysis. The magnetization and ferroelectric polarization are found to be significantly improved in Bi0.85Sm0.1Ho0.05FeO3 than Bi0.9Sm0.1FeO3 and BiFeO3 ceramics. Temperature dependent dielectric constant shows an anomaly at 290° *C* nearer to *TN*, which is due to the intrinsic magnetoelectric coupling of Bi0.85Sm0.1Ho0.05FeO3 ceramic. A clear change in area of *P* - *E* loop after magnetic pooling also conforms the signature of magnetoelectric coupling. Hence it is concluded that, Bi0.85Sm0.1Ho0.05FeO3 is one of the probable candidate in the family of BiFeO3 to enhance magnetoelectric effect at ambient temperature and helpful for device applications.

Acknowledgements

One of the author R. Rajesh would like to thank the following centres:

SAIF, IIT Madras, Department of Nanoscience and Technology, Karunya University, Coimbatore, Department of Physics, Alagappa University , Karaikudi , ACIC, St. Joseph College, Trichy. The author KR acknowledges UGC for emeritus scheme.

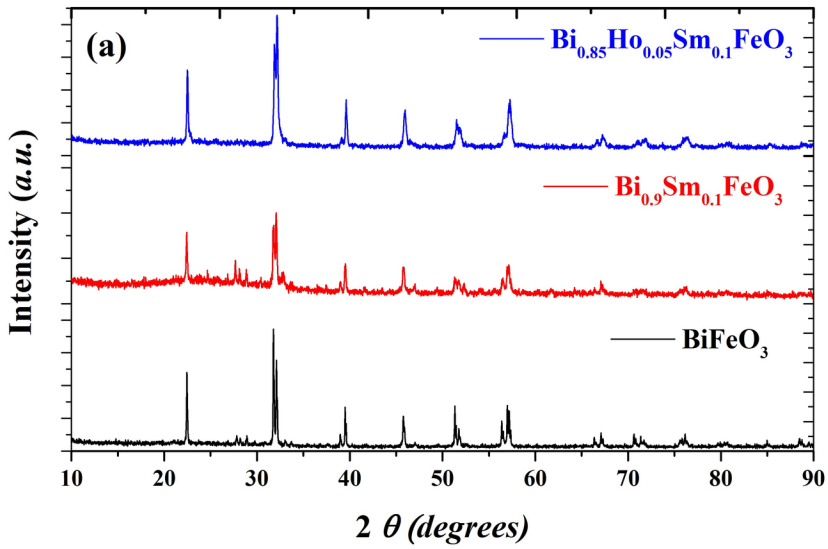

Figure 1: X- ray diffraction of $BiFeO_3$, $Bi_{0.9}Sm_{0.1}FeO_3$ and $Bi_{0.85}$ $Ho_{0.05}$ $Sm_{0.1}FeO_3$.

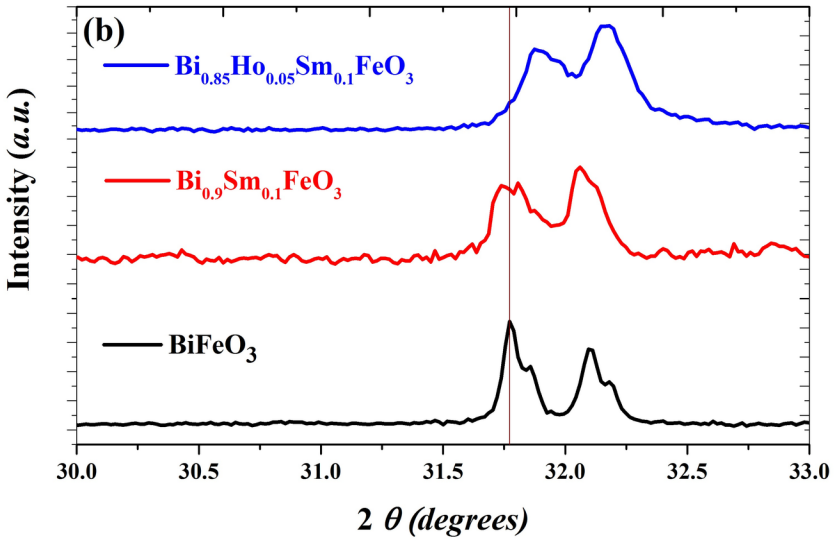

Figure 2: Predominant splitting of (1 0 4) and (1 1 0) planes of $BiFeO_3$, $Bi_{0.9}Sm_{0.1}FeO_3$ and $Bi_{0.85}$ $Ho_{0.05}$ $Sm_{0.1}FeO_3$.

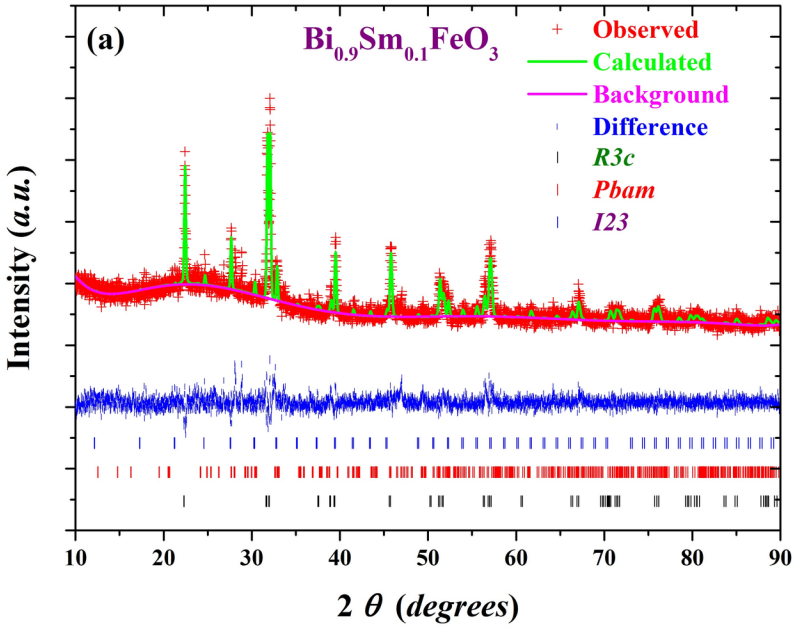

Figure 3: Rietveld refinement of $Bi_{0.9}Sm_{0.1}FeO_3$. The red plus symbols represent the observed data whereas calculated pattern is showed as solid green line. The difference pattern between the calculated and observed data is given as pink solid line. Brown vertical bars represent the allowed Bragg peak positions for their respective crystal structures while the red and green vertical bars indicates secondary phases of the corresponding crystal structure

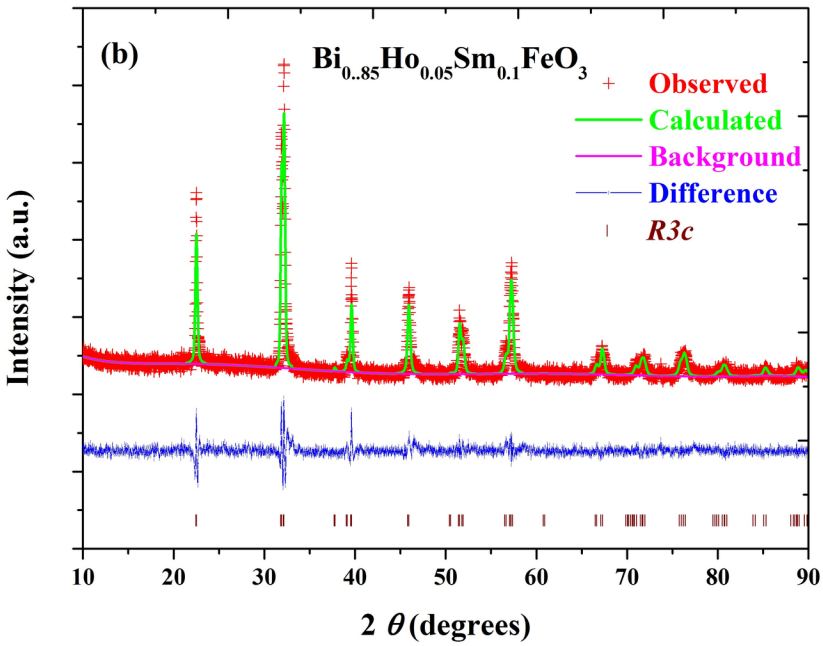

Figure 4: Rietveld refinement of $Bi_{0.85}Ho_{0.05}Sm_{0.1}FeO3$. The red plus symbols represent the observed data whereas calculated pattern is showed as solid green line. The difference pattern between the calculated and observed data is given as pink solid line. Brown vertical bars represent the allowed Bragg peak positions for their respective crystal structures while the red and green vertical bars indicates secondary phases of the corresponding crystal structure

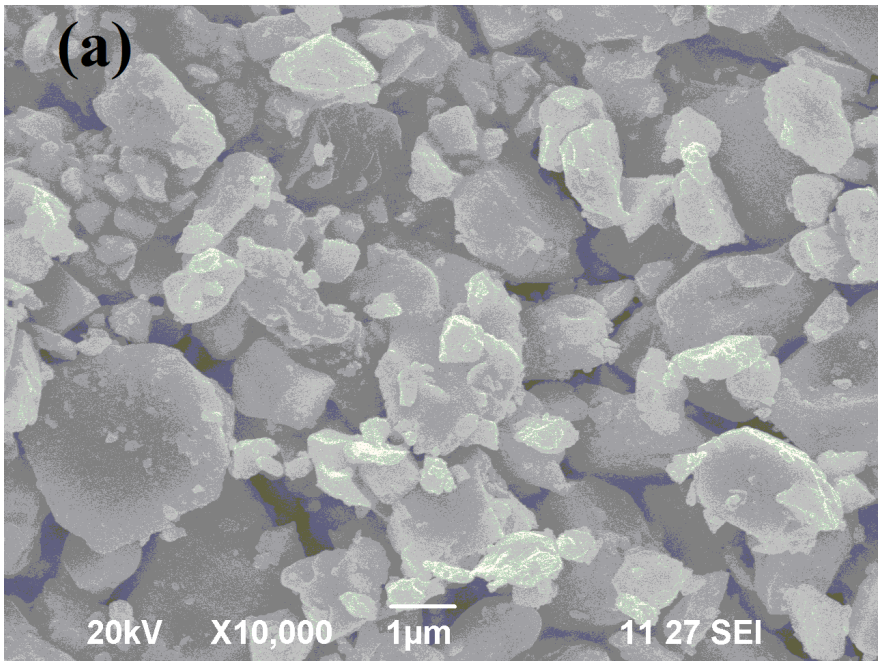

Figure 5: scanning electron micrograph of $BiFeO_3$

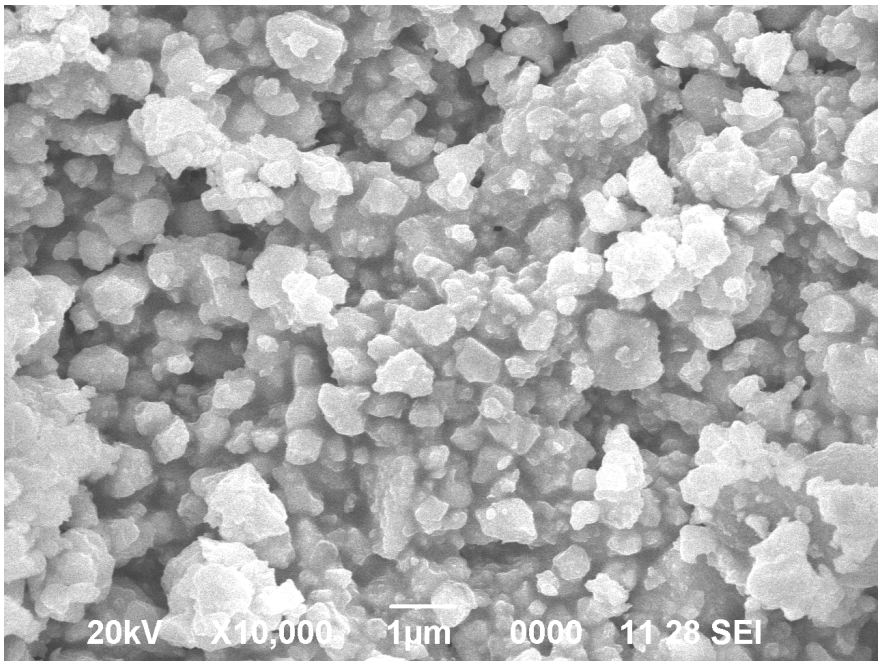

Figure 6: Scanning electron micrograph of $Bi_{0.85}Ho_{0.05}Sm_{0.1}FeO_3$

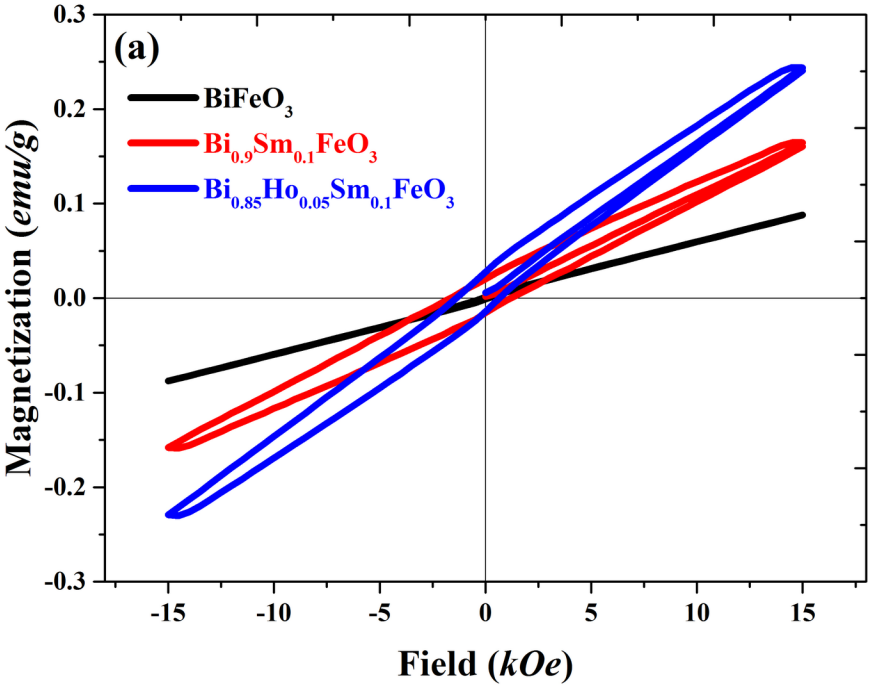

Figure 7: Magnetization as a function of applied field for $BiFeO_3$, $Bi_{0.9}Sm_{0.1}FeO_3$ and $Bi_{0.85}$ $Ho_{0.05}$ $Sm_{0.1}FeO_3$ at ambient temperature

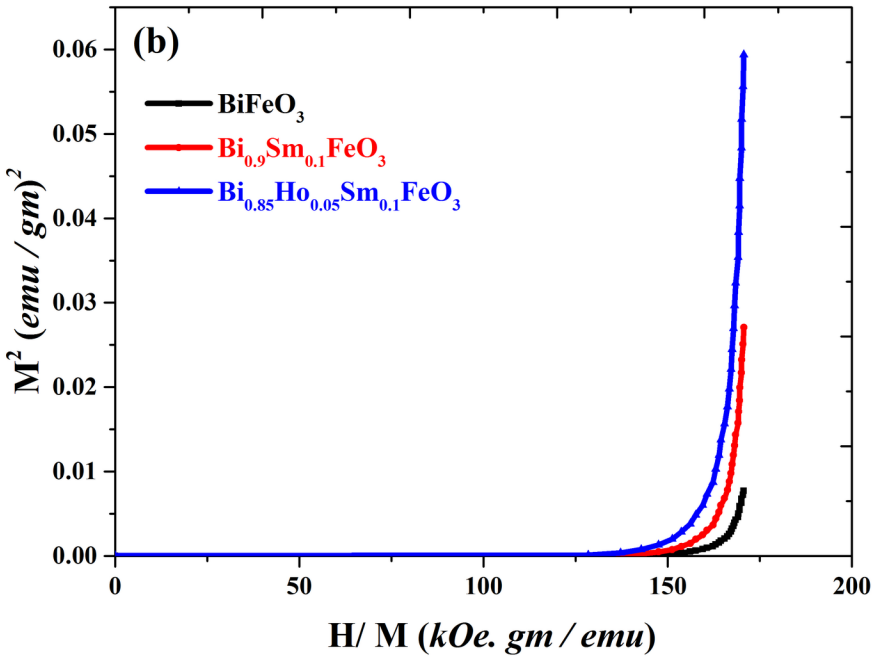

Figure 8: ABK plot of $BiFeO_3$, $Bi_{0.9}Sm_{0.1}FeO_3$ and $Bi_{0.85}$ $Ho_{0.05}$ $Sm_{0.1}FeO_3$ samples at ambient temperature

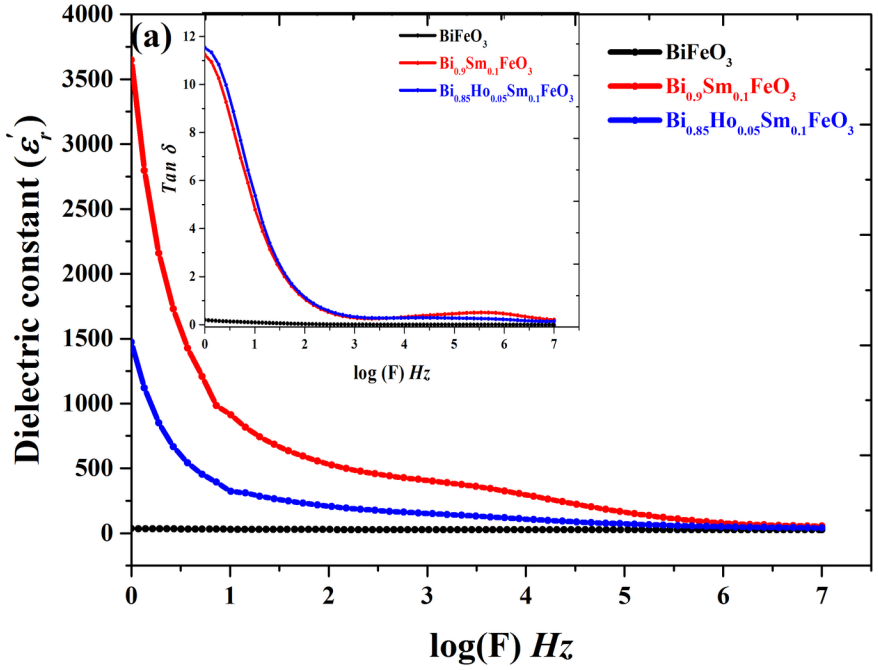

Figure 9: Frequency dependent dielectric constant of $BiFeO_3$, $Bi_{0.9}Sm_{0.1}FeO_3$ and $Bi_{0.85}$ $Ho_{0.05}$ $Sm_{0.1}FeO_3$ at ambient temperature. Inset of Fig is the frequency-dependent dielectric loss of $BiFeO_3$, $Bi_{0.9}Sm_{0.1}$FeO3 and $Bi_{0.85}$ $Ho_{0.05}$ $Sm_{0.1}$FeO3 at ambient temperature.

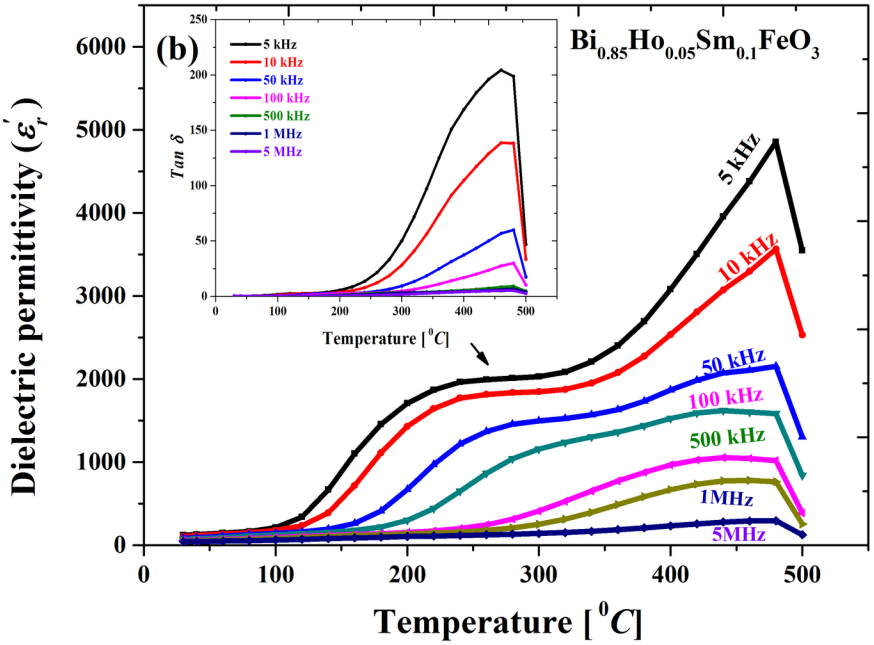

Figure 10: Temperature dependent dielectric constant of $Bi_{0.85}Ho_{0.05}Sm_{0.1}FeO_3$ ceramic between the frequency ranges of 5 *kHz* to 5 *MHz* Dielectric anomaly observed at 290° *C* is indicated by an arrow mark. inset of Fig. shows temperature dependent dielectric loss of $Bi_{0.85}$ $Ho_{0.05}$ $Sm_{0.1}FeO_3$ ceramic between the frequency ranges of 5 *kHz* to 5 *MHz*

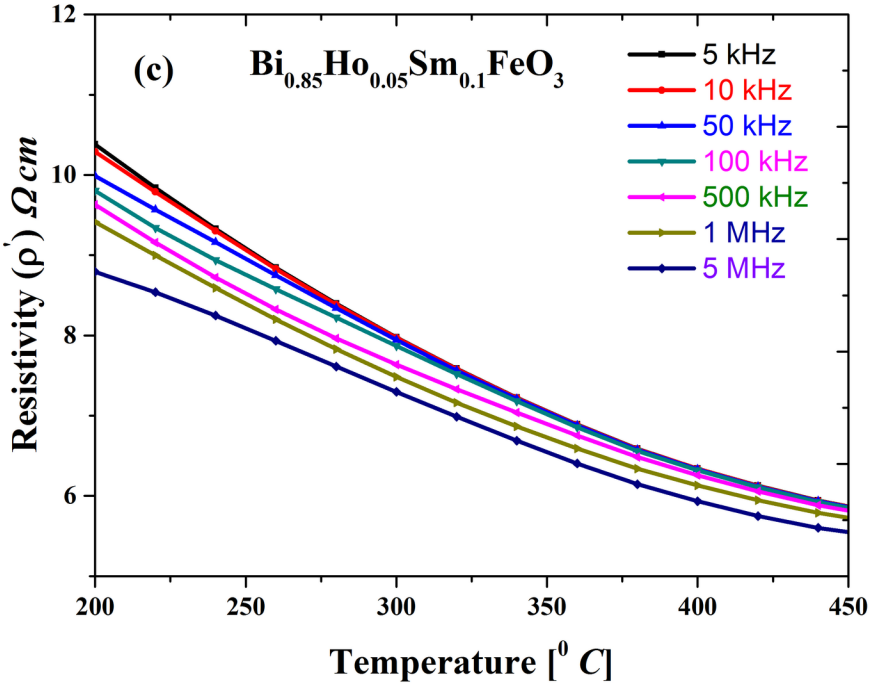

Figure 11: Temperature dependent resistivity of $Bi_{0.85}Sm_{0.1}Ho_{0.05}FeO_3$ ceramic between the frequency ranges of 5 *kHz* to 5 *MHz*

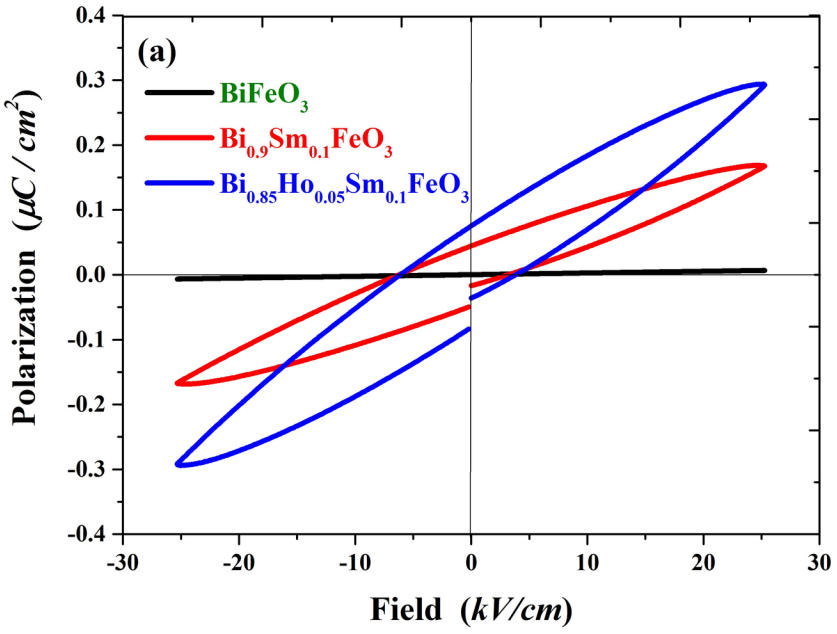

Figure 12: Ferroelectric hysteresis loop of $BiFeO_3$, $Bi_{0.9}Sm_{0.1}FeO_3$ and $Bi_{0.85}$ $Ho_{0.05}$ $Sm_{0.1}FeO_3$ at 100 Hz

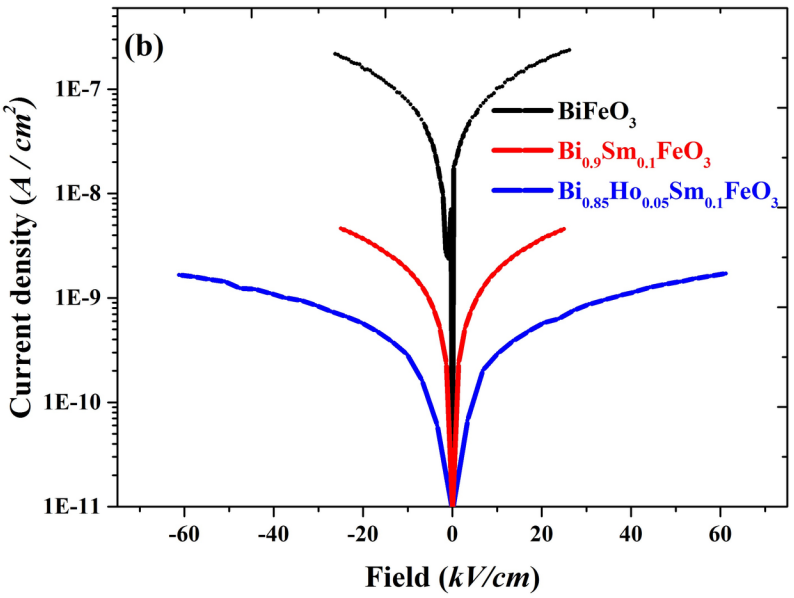

Figure 13: Leakage current density measurements as a function of applied electric field for $BiFeO_3$, $Bi_{0.9}Sm_{0.1}FeO_3$ and $Bi_{0.85}$ $Ho_{0.05}$ $Sm_{0.1}FeO_3$

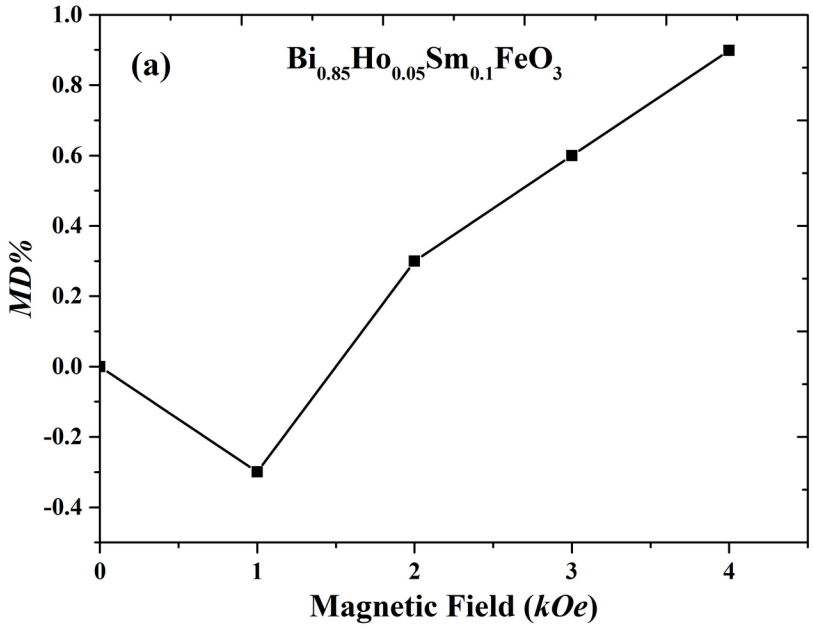

Figure 14: Ambient temperature magnetodielectric effect of $Bi_{0.85}$ $Ho_{0.05}$ $Sm_{0.1}FeO_3$ at 100 *Hz*.

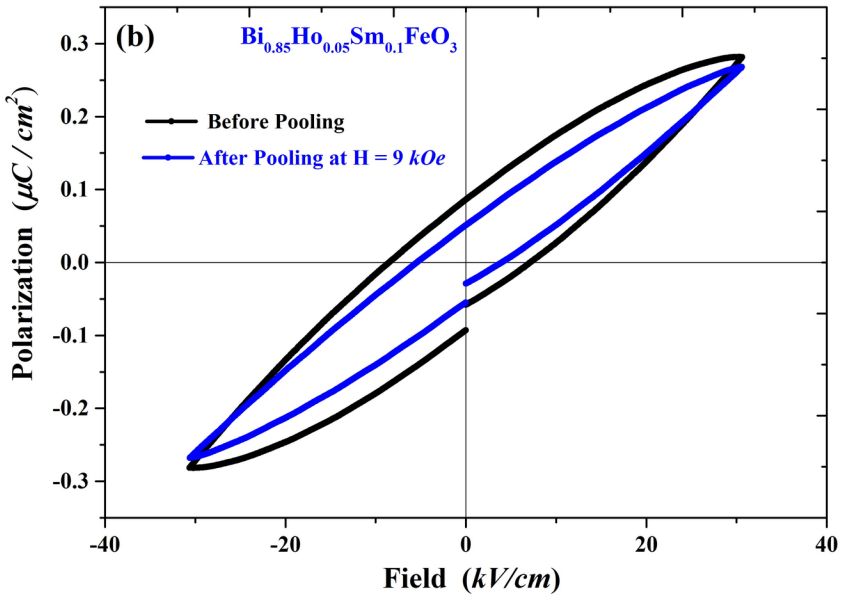

Figure 15: Ferroelectric hysteresis loops of $Bi_{0.85}$ $Ho_{0.05}Sm_{0.1}FeO_3$ ceramic measured at a frequency of 100 *Hz* before and after poling at a dc magnetic field of 9 *kOe* for 25 *minutes*

Sample	$BiFeO_3$	$Bi_{0.9}Sm_{0.1}FeO_3$	$Bi_{0.85}Sm_{0.1}Ho_{0.05}FeO_3$
Lattice Parameters	a = b = 5.58 ; c = 13.86	a = b = 5.57 ; c = 13.84	a = b = 5.57 ; c = 13.83
Interfacial Angles	$\alpha = \beta = 90°$; $\gamma = 120°$	$\alpha = \beta = 90°$; $\gamma = 120°$	$\alpha = \beta = 90°$; $\gamma = 120°$
Atomic position	Bi (0, 0, 0)	Bi / Sm (0, 0, 0)	Bi/Sm/Ho (0, 0, 0)
	Fe (0, 0, 0.22)	Fe (0, 0, 0.22)	Fe (0, 0, 0.22)
	O (0.45, 0.02, 0.95)	O (0.45, 0.02, 0.95)	O (0.43, 0.0, 0.96)
Volume (Å^3)	373.39	371.96	372.11
Bragg reflection ratio			
$BiFeO_3$ ***(R3c)***	0.85	0.92	1
$Bi_2Fe_4O_9$ ***(Pbam)***	0.14	0.03	
$Bi_{25}FeO_{40}$ ***(I23)***	0.01	0.05	
Density (***gm / cm^3***)	8.35	8.22	8.16
Bond angle (Fe_1 **- O -** Fe_2)	155.13°	155.13°	156.13
Bond length (Fe – O_1)	1.96	1.96	1.92
Bond length (Fe – O_2)	2.1	2.1	2.13
R - Factors	wRp = 0.17	wRp = 0.13	wRp = 0.13
	$R_F^2 = 0.24$	$R_F^2 = 0.51$	$R_F^2 = 0.16$
	$R_b = 0.14$	$R_b = 0.17$	$R_b = 0.14$
Goodness of fit (GOF)	1.24	1.08	1.21

Table 1: Rietveld refinement of $BiFeO_3$, $Bi_{0.9}Sm_{0.1}FeO_3$ and $Bi_{0.85}$ $Ho_{0.05}$ $Sm_{0.1}FeO_3$

References

Z. Abdelkafi, G. Khasskhoussi, and N. Abdelmoula. Dielectric Relaxation Study of Multiferroic BiFe0.95(Ni0.5Ti0.5)0.05O3. *Journal of Electronic Materials*, 47(3):2017–2024, dec 2017. doi: 10.1007/s11664-017-6003-x. URL https://doi.org/10.1007%2Fs11664-017-6003-x.

L. Benguigui. Thermodynamic theory of the morphotropic phase transition tetragonal-rhombohedral in the perovskite ferroelectrics. *Solid State Communications*, 11(6):825–828, sep 1972. doi: 10.1016/0038-1098(72)90280-3. URL https://doi.org/10.1016%2F0038-1098%2872%2990280-3.

G. Catalan. Magnetocapacitance without magnetoelectric coupling. *Applied Physics Letters*, 88(10):102902, mar 2006. doi: 10.1063/1.2177543. URL https://doi.org/10.1063%2F1.2177543.

Gustau Catalan and James F. Scott. Physics and Applications of Bismuth Ferrite. *Advanced Materials*, 21(24):2463–2485, jun 2009. doi: 10.1002/adma.200802849. URL https://doi.org/10.1002%2Fadma.200802849.

Tapan Chatterji, Bachir Ouladdiaf, P. Mandal, B. Bandyopadhyay, and B. Ghosh. Jahn-Teller transition inLa1-xSrxMnO3in the low-doping region(0x˜0.1). *Physical Review B*, 66(5), aug 2002. doi: 10.1103/physrevb.66.054403. URL https://doi.org/10.1103%2Fphysrevb.66.054403.

Haiyang Dai, Tao Li, Zhenping Chen, Dewei Liu, Renzhong Xue, Chengzhou Zhao, Haizeng Liu, and Ningkang Huang. Studies on the structural electrical and magnetic properties of Ce-doped BiFeO 3 ceramics. *Journal of Alloys and Compounds*, 672:182–189, jul 2016. doi: 10.1016/j.jallcom.2016.02.134. URL https://doi.org/10.1016%2Fj.jallcom.2016.02.134.

Anton Gagin and Igor Levin. Accounting for unknown systematic errors in Rietveld refinements: a Bayesian statistics approach. *Journal of Applied Crystallography*, 48(4):1201–1211, jul 2015. doi: 10.1107/s1600576715011322. URL https://doi.org/10.1107%2Fs1600576715011322.

Shahzad Hussain, S.K. Hasanain, G. Hassnain Jaffari, Naveed Zafar Ali, M. Siddique, and S. Ismat Shah. Correlation between structure oxygen content and the multiferroic properties of Sr doped BiFeO3. *Journal of Alloys and Compounds*, 622:8–16, feb 2015. doi: 10.1016/j.jallcom.2014.10.029. URL https://doi.org/10.1016%2Fj.jallcom.2014.10.029.

S. Jangid, S.K. Barbar, Indu Bala, and M. Roy. Structural thermal, electrical and magnetic properties of pure and 50% La doped BiFeO3 ceramics. *Physica B: Condensed Matter*, 407(18):3694–3699, sep 2012. doi: 10.1016/j.physb.2012.05.013. URL https://doi.org/10.1016%2Fj.physb.2012.05.013.

T. Karthik, A. Srinivas, V. Kamaraj, and V. Chandrasekeran. Influence of in-situ magnetic field pressing on the structural and multiferroic behaviour of BiFeO3 ceramics. *Ceramics International*, 38(2):1093–1098, mar 2012. doi: 10.1016/j.ceramint.2011.08.036. URL https://doi.org/10.1016%2Fj.ceramint.2011.08.036.

V.A. Khomchenko, J.A. Paixão, V.V. Shvartsman, P. Borisov, W. Kleemann, D.V. Karpinsky, and A.L. Kholkin. Effect of Sm substitution on ferroelectric and magnetic properties of BiFeO3. *Scripta Materialia*, 62(5):238–241, mar 2010. doi: 10.1016/j.scriptamat.2009.11.005. URL https://doi.org/10.1016%2Fj.scriptamat.2009.11.005.

Amit Kumar and K.L. Yadav. Enhanced magnetodielectric properties of single-phase Bi0.95-xLa0.05LuxFeO3 multiferroic system. *Journal of Alloys and Compounds*, 554:138–141, mar 2013. doi: 10.1016/j.jallcom.2012.11.189. URL https://doi.org/10.1016%2Fj.jallcom.2012.11.189.

Pawan Kumar, Nisha Shankhwar, A. Srinivasan, and Manoranjan Kar. Oxygen octahedra distortion induced structural and magnetic phase transitions in Bi1-xCaxFe1-xMnxO3 ceramics. *Journal of Applied Physics*, 117(19):194103, may 2015. doi: 10.1063/1.4921433. URL https://doi.org/10.1063%2F1.4921433.

Jinhua Mao, Yu Sui, Xianjie Wang, Yiyun Yang, Xingquan Zhang, Yang Wang, Yi Wang, and Wanfa Liu. Spin-glass behavior and exchange bias in phase-separated Nd0.85Sr0.15CoO3. *Journal of Alloys and Compounds*, 509

(15):4950–4953, apr 2011. doi: 10.1016/j.jallcom.2011.01.105. URL https://doi.org/10.1016%2Fj.jallcom.2011.01.105.

M. Muneeswaran, Radhalayam Dhanalakshmi, and N. V. Giridharan. Effect of Tb substitution on structural optical, electrical and magnetic properties of BiFeO3. *Journal of Materials Science: Materials in Electronics*, 26(6):3827–3839, mar 2015. doi: 10.1007/s10854-015-2909-3. URL https://doi.org/10.1007%2Fs10854-015-2909-3.

C. Nayek, A. Tamilselvan, Ch. Thirmal, P. Murugavel, and S. Balakumar. Origin of enhanced magnetization in rare earth doped multiferroic bismuth ferrite. *Journal of Applied Physics*, 115(7):073902, feb 2014. doi: 10.1063/1.4865958. URL https://doi.org/10.1063%2F1.4865958.

V. R. Palkar, Darshan C. Kundaliya, S. K. Malik, and S. Bhattacharya. Magnetoelectricity at room temperature in theBi0.9-xTbxLa0.1FeO3system. *Physical Review B*, 69(21), jun 2004. doi: 10.1103/physrevb.69.212102. URL https://doi.org/10.1103%2Fphysrevb.69.212102.

Samita Pattanayak, R. N. P. Choudhary, and Piyush R. Das. Effect of Gd-substitution on phase transition and conduction mechanism of BiFeO3. *Journal of Materials Science: Materials in Electronics*, 24(8):2767–2771, mar 2013. doi: 10.1007/s10854-013-1168-4. URL https://doi.org/10.1007%2Fs10854-013-1168-4.

T. Durga Rao, T. Karthik, Adiraj Srinivas, and Saket Asthana. Study of structural magnetic and electrical properties on Ho-substituted BiFeO3. *Solid State Communications*, 152(23):2071–2077, dec 2012. doi: 10.1016/j.ssc.2012.08.007. URL https://doi.org/10.1016%2Fj.ssc.2012.08.007.

Benjamin Ruette, S. Zvyagin, A. P. Pyatakov, A. Bush, J. F. Li, V. I. Belotelov, A. K. Zvezdin, and D. Viehland. Magnetic-field-induced phase transition inBiFeO3observed by high-field electron spin resonance: Cycloidal to homogeneous spin order. *Physical Review B*, 69(6), feb 2004. doi: 10.1103/physrevb.69.064114. URL https://doi.org/10.1103%2Fphysrevb.69.064114.

Prakash Chandra Sati, Manisha Arora, Sunil Chauhan, Manoj Kumar, and Sandeep Chhoker. Effect of Dy substitution on structural magnetic and optical properties of BiFeO3 ceramics. *Journal of Physics and Chemistry of Solids*, 75(1):105–108, jan 2014. doi: 10.1016/j.jpcs.2013.09.003. URL https://doi.org/10.1016%2Fj.jpcs.2013.09.003.

K. SINGH, S. A. BAND, and W. K. KINGE. Effect of Sintering Temperature on Dielectric Properties of Pb(Fe1/2Nb1/2)O3Perovskite Material. *Ferroelectrics*, 306(1):179–185, jan 2004. doi: 10.1080/00150190490460821. URL https://doi.org/10.1080%2F00150190490460821.

Rohit Singh, Saurabh Kumar Srivastava, Arun K. Nigam, Vladimir V. Khovaylo, Lajos K. Varga, and Ratnamala Chatterjee. Use of Arrott plots to identify Néel temperature (TN) in metamagnetic Ni48Co6Mn26Al20 polycrystalline ribbons. *Journal of Applied Physics*, 114(24):243911, dec 2013. doi: 10.1063/1.4858377. URL https://doi.org/10.1063%2F1.4858377.

Pittala Suresh, P.D. Babu, and S. Srinath. Role of (La Gd) co-doping on the enhanced dielectric and magnetic properties of BiFeO 3 ceramics. *Ceramics International*, 42(3):4176–4184, feb 2016. doi: 10.1016/j.ceramint.2015.11.091. URL https://doi.org/10.1016%2Fj.ceramint.2015.11.091.

Patri Tirupathi and Amreesh Chandra. Stabilization of dielectric anomaly near the magnetic phase transition in Ca2+ doped BiFeO3 multifunctional ceramics. *Journal of Alloys and Compounds*, 564:151–157, jul 2013. doi: 10.1016/j.jallcom.2013.02.095. URL https://doi.org/10.1016%2Fj.jallcom.2013.02.095.

Brian H. Toby and Robert B. Von Dreele. GSAS-II: the genesis of a modern open-source all purpose crystallography software package. *Journal of Applied Crystallography*, 46(2):544–549, mar 2013. doi: 10.1107/s0021889813003531. URL https://doi.org/10.1107%2Fs0021889813003531.

P Uniyal and K L Yadav. Pr doped bismuth ferrite ceramics with enhanced multiferroic properties. *Journal of Physics: Condensed Matter*, 21(40):405901, sep 2009. doi: 10.1088/0953-8984/21/40/405901. URL https://doi.org/10.1088%2F0953-8984%2F21%2F40%2F405901.

S. T. Zhang, M. H. Lu, D. Wu, Y. F. Chen, and N. B. Ming. Larger polarization and weak ferromagnetism in quenched BiFeO3 ceramics with a distorted rhombohedral crystal structure. *Applied Physics Letters*, 87(26):262907, dec 2005. doi: 10.1063/1.2147719. URL https://doi.org/10.1063%2F1.2147719.

Xingquan Zhang, Yu Sui, Xianjie Wang, Jinhua Mao, Ruibin Zhu, Yi Wang, Zhu Wang, Yuqiang Liu, and Wanfa Liu. Multiferroic and magnetoelectric properties of single-phase Bi0.85La0.1Ho0.05FeO3 ceramics. *Journal of Alloys and Compounds*, 509(19):5908–5912, may 2011. doi: 10.1016/j.jallcom.2011.03.037. URL https://doi.org/10.1016%2Fj.jallcom.2011.03.037.